Performance Comparison of Tetrolet Transform and Wavelet-Based Transforms for Medical Image Denoising

Murat Ceylan[1], Ayşe Elif Canbilen[1*]

Abstract: Noise reduces the quality of medical images and raise the difficulties of diagnosis. Although the wavelet transform has already been used in medical noise removal applications extensively, there are many other multi-resolution analysis methods proposed in recent years for denoising. The main goal of this study is comparing the image denoising abilities of some of these methods with wavelet transform. In this paper, image denoising is implemented by a three-stage methodology. Effectiveness of the multiresolution analysis methodologies has been investigated for standard test images beside magnetic resonans, mammography and fundus images. Performances of the transforms are compared by using peak signal to noise ratio, mean square error, mean structural similarity index and feature similarity index. The best results are obtained by tetrolet transform for random and rician noises with the benchmark images. Medical image denoising performance of Tetrolet transform is compared to other multi resolution analysis methods for the first time in the literature with this study. It surpassed ridgelet and haar wavelet transforms while the noise ratio was low. On the other hand, it is seen that curvelet transforms are effectively produce the best results for all rates of noise on medical images.

1. Introduction

The main argument of image processing, Fourier analysis, is inadequate to solve denoising problems because it is not able to determine the time of frequency changes. Wavelet transform (WT) was proposed to overcome this problem [1,2]. Although it is a popular method for processing medical images [3-6], it suffers from limited direction.

Ridgelet transform (RT) uses angular windows instead of directional implementation of WT [7]. Although RT was used for denoising [8,9], it is not good enough for denoising medical images [10,11].

Curvelet transform (CT) that uses curves instead of lines for windowing was improved [12-14]. Since CT is efficiently detects edge information of images, it is commonly used for denoising [15-17]. Ma and Plonka [18], presented a review on CT including its evolution history, theory and its correlation to other multi-resolution methods. CT is implemented on a variety of medical images for segmenting and denoising and had efficient results [19,20]. Raju and Kumar [21] also compared denoising performances of dual tree complex WT and CT on medical images and CT had better results.

Tetrolet transform (TT) was came out as a new generation multi-resolution method [22]. In this local analysis method, image regions are rearranged according to five different shapes called tetrominoes and haar WT is implemented on these regions. WT and TT are compared for denoising of benchmark images and realized that TT is superior than WT [23,24]. Ceylan and Öztürk [25], studied on optimizing the tetrominoe combinations in denoising algorihms and shortened the process time. There is no study which compares the denoising performance of TT with the other transforms (RT and CT) in the literature.

Although the most frequent noise type of medical images is gaussian [26], MR images follow a rician distribution [27-28]. So, recent studies about medical image denoising focus on removing gaussian and rician noise [29-30].

In this paper, we perform denoising on medical and standard test images. We removed the artificially implemented noise by using different multi-resolution analysis (MRA) methods and evaluated and compared the performance of each method. Thisis the first paper introducing Tetrolet transform into comparative medical image denoising systems.

2. Materials and Methods

MRA techniques in this study, are given in Section 2.1. Noise addition and thresholding methods are included in Section 2.2. Performance evaluation methods are given in Section 2.3.

2.1. Multiresolution Analysis (MRA) Methods

2.1.1. Wavelet Transform (WT)

WT is the basis form of the MRA and has been implemented for many years. Generally, daubechies wavelets (especially db4) are preferred for denoising algorithms in literature [23, 31].
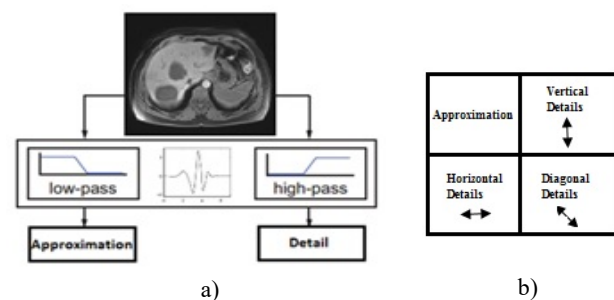
Fig. 1. WT application to an image: (a) one level two-dimensional (2D) WT, (b) coefficient matrix of WT obtained by decomposition level.

[1] *Electr. and Electro. Eng., Selcuk University, Konya – 42075, TURKEY*
[*] *Corresponding Author: Email: ayseelif@selcuk.edu.tr*

We use db4 and also haar wavelet to the images to decide whether TT, as a haar WT based method, surpasses haar WT or not. WT coefficient matrix of an image is computed as implementing discrete form of WT to rows and columns as seen in Fig. 1(a). At the end of the WT decomposition level, an approximation and three detail components are obtained and located in the coefficient matrix as seen in Fig. 1(b).

2.1.2. Tetrolet Transform (TT)

Tetrolet transform (TT) is an effective, local and scalable algorithm. In order to implement TT, image matrix is first separated into blocks each of which include 4x4 pixels. If the image size cannot be divided by four, zero-padding should be applied. There are five shapes called tetrominoes which of each contain four pixels, are used for TT (Fig. 2. (a)). Four of them are chosen and the selected tetrominoes should be located into a 4x4 sized pixel blocks. 117 different combinations are possible and one

of them is given in Fig. 2. (b). After locating the tetrominoes, pixels of the 4x4 sized blocks are rearranged according to TT rules with the selected combination of tetrominoes and haar WT is applied on the reformed part of the image locally. This procedure is applied on whole 4x4 blocks in the image. At the end of the decomposition level, a coefficient matrix whose size is the same as the original image is obtained (Fig. 3).

Fig. 2. Tetrominoes: (a) shapes of the tetrominoes, (b) a combination of tetrominoes for a 4x4 pixel block.
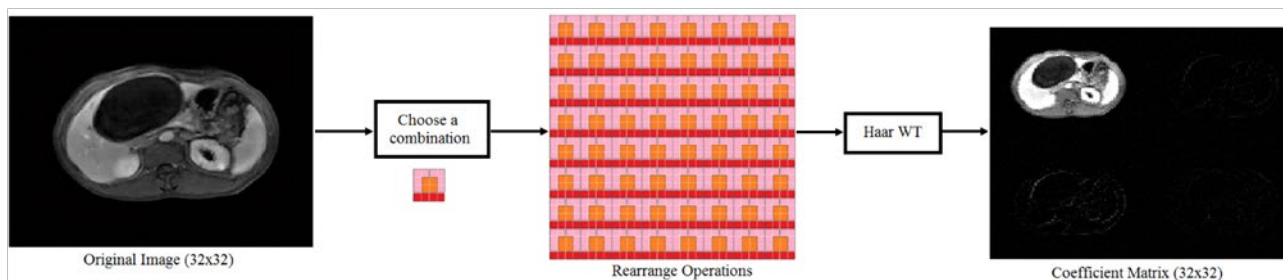
Fig. 3. Decomposition steps of TT

2.1.3. Ridgelet Transform (RT)

Poor directionality of WT is overcame with RT by using an angle parameter. This method is successful at catching one-dimensional (1D) line singularities in multi-dimensional signals like images. RT is based on radon transform (RAT). So, it is possible to comprehend RT by understanding RAT. Mathematical background of RAT is given in [9, 13]. The finite RAT of an image $x(i,j)$ is given as follows where $L_{k,l}$ represents the lines and y_0 is the local mean:

$$r_k[l] = \sum_{(i,j) \in L_{k,l}} [x(i,j) - y_0] \qquad (1)$$

Finite RT is defined by performing 1D WT to matrix $r_k[l]$, column by column [8]. As another way, RT can be achieved in Fourier domain by using 2D fast Fourier transform (FFT) [11]. Initially 2D FFT is applied, after that Fourier coefficients are interpolated along lines which pass through the frequency space and 1D reverse FFT is calculated. Finally, 1D WT is applied and RT coefficients matrix of the image is obtained (Fig. 4).
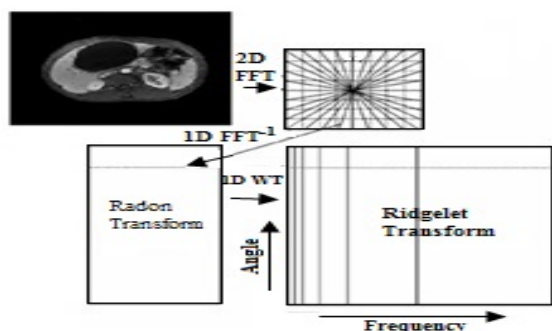

Fig. 4. RT application to an image.

2.1.4. Curvelet Transform (CT)

Curvelet transform (CT) that combines MRA with parabolic scaling is enhanced by improving RT. It has the ability of catching quadratic curves on images. In order to apply CT, firstly the image is decomposed into different scaled subbands. Then, each subband is windowed into squares and each square is renormalized [15]. Lastly, discrete RT is applied on each square (Fig. 5).
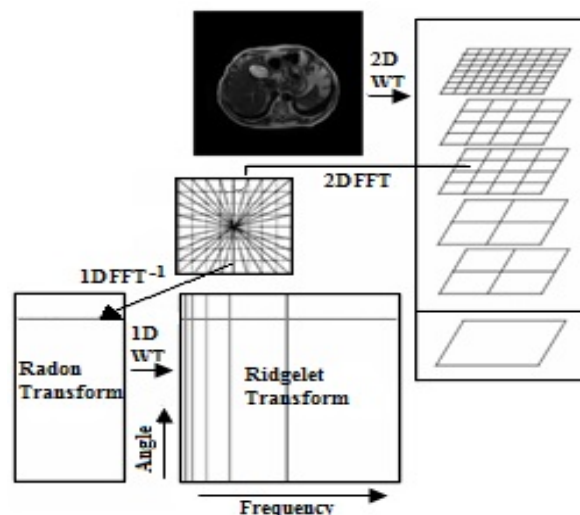

Fig. 5. CT application to an image.

There are two generations of CT. First one is efficiently used on images for denoising but its process takes a long time compared to second generation [14]. First generation CT (FGCT) based on RT is limited in digital application because of the geometry of ridgelets [18]. On the other hand, second generation CT (SGCT- fast

discrete CT) uses unequally-spaced FFT and wrapping (Fig. 6). Thus, fast discrete CT can be implemented faster, less redundantly and simpler than FGCT [14].
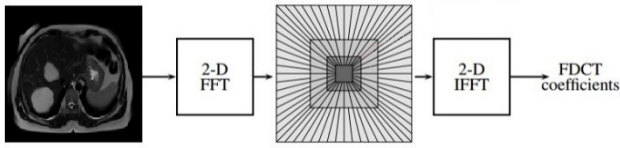

Fig. 6. Second generation (fast discrete) CT (SGCT) scheme.

2.2. Noise Addition and Thresholding Methods

In this study, random, gaussian and rician noise are applied on all the medical and test images.

We applied random noise (N_r) to the images with Eq. (2). Here, *sigma* is the noise ratio which is an important factor to specify the amount of noise.

$$X_n = X + sigma * N_r$$

The gaussian distribution of a random variable x, could be defined as follows [30]:

$$P(x) = \frac{1}{\sigma\sqrt{2\pi}} e^{\frac{-(x-\mu)^2}{2\sigma^2}} \tag{2}$$

where $x = (-\infty, \infty)$, μ is mean and σ is standard deviation. Additionally, if m is the pixel intensity of the noisy image and s is the pixel intensity of noiseless image, while Γ_0 represents the modified order of the first kind of Bessel function, the rician probability distribution for m is given by [28, 30]

$$P(m) = \frac{m^2}{\sigma^2} e^{\frac{-(s^2 + m^2)}{2\sigma^2}} \Gamma_0(s\frac{m^2}{\sigma^2}) \tag{3}$$

In our study, we used three *sigma* values for random noise and three signal to noise ratios (snr) for gaussian and rician noise. The main difference between random, rician and gaussian noise, is that gaussian noise is inversely proportional with snr value. So, if snr increases, noise ratio decreases for gaussian.

A thresholding process is implemented on detail coefficients obtained by transforms. We used universal and hard thresholding methods. The threshold value T in universal thresholding is given by:

$$T = \sigma\sqrt{2\log(M)} \tag{4}$$

where M is the size of the image and σ^2 is the noise variance. In hard thresholding, if absolute value of a coefficient is greater than the specified threshold value, it remains unchanged. However, if the value is less than the threshold, it is supposed to be zero:

$$\hat{X} = sign(Y)(Y.*(abs(Y) > T)) \tag{5}$$

where $\hat{X}$ represents the calculated coefficients, Y states the noisy coefficients and T is the threshold.

2.3. Performance Measurement

Each implemented process causes corruptions on images. The purpose of denoising algorithms is reconstructing images with minimum decay. In order to compare performances of the MRA methods, we have calculated PSNR, MSE, MSSIM and FSIM values for each image.

2.3.1. Mean Square Error (MSE)

The square of the numeric difference between two images is calculated. Lower MSE means cleaner image. While R and C state number of rows and columns of images x and y, MSE is denoted as:

$$MSE(x,y) = \frac{1}{RC} . \sum_{i=1}^{R} \sum_{j=1}^{C} (x_{i,j} - y_{i,j})^2 \tag{6}$$

2.3.2. Peak Signal to Noise Ratio (PSNR)

It is an objective performance test which ensures to score lost information in dB. Higher PSNR means less decay. Considering x is the original image and y is the obtained image, PSNR is denoted as:

$$PSNR(x,y) = 10.\log_{10}(255^2 / MSE(x,y)) \tag{7}$$

2.3.3. Mean Structural Similarity Index (MSSIM)

Recently, MSSIM has begun to be used extensively in image/video processing applications through its simple process as an alternative of MSE [32].

SSIM combines three components called luminance distortion term $l(x,y)$, contrast distortion term $c(x,y)$ and correlation term $s(x,y)$ [33]. SSIM of the two images are calculated as given in Eq. (9), where and are the similarity maps. It can take values between [-1, 1] and if $SSIM(x,y) = 1$, it means the given images are the same. It is applied on local regions using a sliding window [34]. This procedure is implemented from top-left to bottom-right corner of the images till all image is operated. MSSIM is denoted as Eq. (10) while is the number of windows:

$$SSIM(x,y) = S_1(x,y).S_2(x,y) \tag{8}$$

$$MSSIM(X,Y) = \frac{1}{M}\sum_{j=1}^{M} SSIM(x_j, y_j) \tag{9}$$

2.3.4. Feature Similarity Index (FSIM)

Another novel performance evaluation method is FSIM. It is calculated by using phase congruence $(PC_m(x))$ and a specified similarity measure $(S_L(x))$ while Ω states the whole image (Eq. (11)). Mathematical background could be find in [35].

$$FSIM = \frac{\sum_{x\in\Omega} S_L(x).PC_m(x)}{\sum_{x\in\Omega} PC_m(x)} \tag{10}$$

3. Experimental Results

In this study, we use five test images and ninety biomedical images which of size is 256x256. Firstly, they are corrupted by noise artificially. Then coefficient matrices are obtained for each image, separately. A thresholding procedure is applied on high frequency components and then images are reconstructed. Finally, the reconstructed and the original images are compared by the performance evaluation criteria (Fig. 7).

Singh [23] came up with the idea of decreasing numbers of tetrominoe orders used for denoising could be shorten the operation time of TT and proposed to use 65 combinations of tetrominoes instead of 117. We also research whether 65 is an optimal number or not for our images. TT is implemented to the noisy images by using an increasing number of tetrominoe combinations from 1 to 117 for each noise ratio and PSNR values

are calculated. It is seen that using all combinations is unnecessary, because the PSNR takes a constant value when number of combinations increases as similar to [25]. So, optimal numbers of

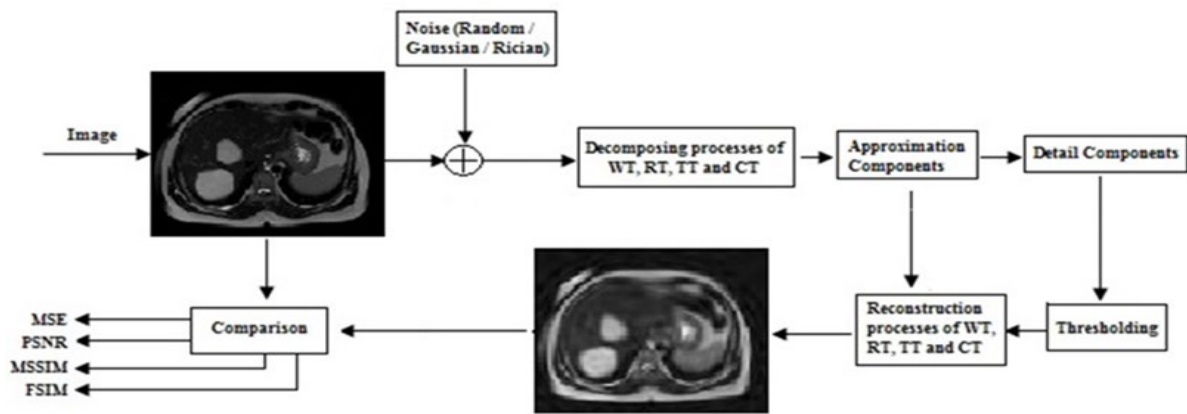combinations are specified for different noise rates and given in Table 1.

Fig. 7. Scheme of denoising process.

Table 1 Optimal number of tetrominoes for benchmark images.

Type of the Images	Noise Type and Ratio								
	Random			Gaussian			Rician		
	5	10	15	3	5	10	3	5	10
Benchmark	30	30	30	65	65	65	37	37	40
Liver MR	40	40	40	40	40	40	40	40	45
Mammography	40	40	40	80	60	37	45	45	45
Fundus	40	40	40	65	65	40	45	45	45

Optimum decomposition level is determined as two for WT and one for TT. Optimal scale number is specified as four for both RT and CT. Sample denoised images for different kinds of noise, are given in Fig. 8. (a)-(d).

Performance test results of benchmark images are given in Table 2. The best results are in bold. Three different image sets are used to have an objective decision about medical image denoising performances of the MRA methods.
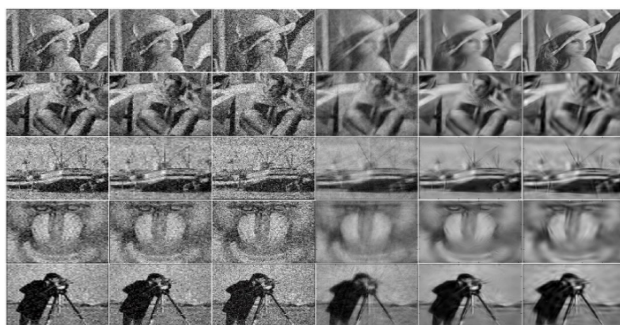
a)
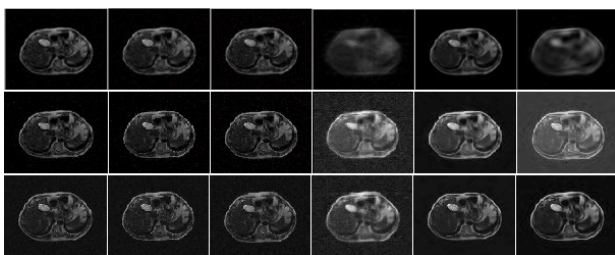
b)
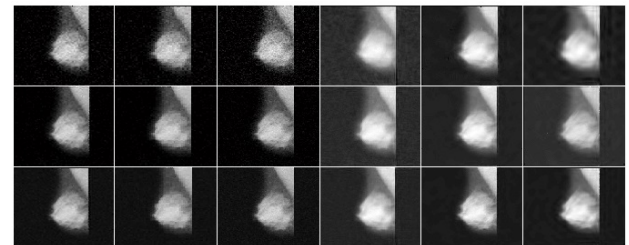
c)
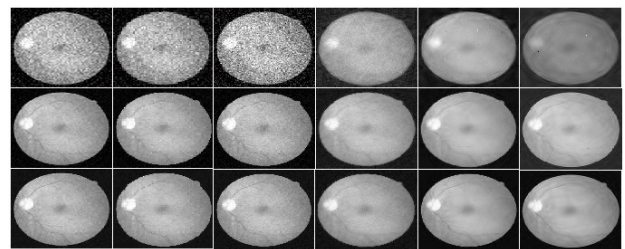
d)

Fig. 8. Sample images denoised by different methods. First column: WT with db4 wavelet, second column: WT with haar wavelet, third column:TT, fourth column: RT, fifth column: FGCT, sixth column: SGCT (a) Benchmark images for gaussian noise (snr=3); (b-d) Medical images (liver MR, mammography and retinal images, respctively). First row: for gaussian noise (snr=3), second row: for random noise (sigma=20), third row: rician noise (snr=15).

Liver MR images were taken from Selcuk University Faculty of Medicine (Department of Radiology), mammography images were taken from MIAS database [36] and fundus images were taken from DRIVE database [37].The evaluation criteria are calculated for all noisy medical images to compare the performances of the methods. The averaged results of the image sets are given in Table 3-5 for each noise ratio, separately. The best results are in bold.

Table 2 Averaged PSNR, MSE, MSSIM, FSIM evaluation criteria values of five benchmark images.

| Type of Noise | Noise Ratio | Evaluation Criteria | Ridgelet | Tetrolet | Wavelet | | Curvelet | |
					Haar	Db4	First Generation	Second Generation
Random	*Sigma* = 5	PSNR	31,52	**35,37**	34,19	34,25	31,43	32,72
		MSE	45,91	**17,79**	22,95	22,73	67,5	35,84
		MSSIM	0,85	**0,95**	0,92	0,93	0,88	0,92
		FSIM	0,94	**0,97**	**0,97**	**0,97**	0,94	0,96
	Sigma = 10	PSNR	26,75	**30,53**	29,1	29,32	28,5	28,21
		MSE	141,26	**57,08**	78,79	76,16	115,18	105,57
		MSSIM	0,71	**0,87**	0,83	0,84	0,82	0,84
		FSIM	0,88	**0,94**	0,92	0,92	0,9	0,92
	Sigma = 15	PSNR	24,84	**27,92**	26,69	26,89	26,85	26,29
		MSE	223,67	**107,78**	154,09	145,61	161,24	169,7
		MSSIM	0,62	**0,79**	0,75	0,76	0,77	0,77
		FSIM	0,84	**0,9**	0,87	0,88	0,87	0,88
Gaussian	*Snr* = 3	PSNR	20,32	21,01	21,13	21,28	**21,73**	21
		MSE	619,33	1177	805,62	709	**454,02**	536,45
		MSSIM	0,38	0,32	0,31	0,35	**0,53**	0,5
		FSIM	0,69	0,62	0,59	0,68	**0,71**	0,67
	Snr = 5	PSNR	20,96	21,3	21,33	21,78	**22,42**	21,92
		MSE	537,78	673,84	641,62	553,74	**392,06**	442,04
		MSSIM	0,39	0,41	0,37	0,42	**0,57**	0,54
		FSIM	0,72	0,69	0,62	0,72	**0,74**	0,72
	Snr = 10	PSNR	21,87	22,78	22,29	22,63	**23,41**	22,88
		MSE	441,47	432,63	495,54	428,4	**320,38**	362,97
		MSSIM	0,45	0,52	0,46	0,5	**0,62**	0,59
		FSIM	0,75	0,76	0,67	0,75	**0,77**	0,76
Rician	*Snr* = 3	PSNR	32,59	37,12	**38,28**	38,26	33,54	33,28
		MSE	35,83	12,48	**8,78**	8,85	49,73	31,58
		MSSIM	0,88	0,97	**0,99**	**0,99**	0,91	0,93
		FSIM	0,96	**0,98**	0,96	0,96	0,95	0,96
	Snr = 5	PSNR	31,51	**34,94**	34,19	34,26	31,42	32,68
		MSE	46,07	**20,5**	22,93	22,71	67,52	36,46
		MSSIM	0,85	0,95	**0,97**	**0,97**	0,88	0,92
		FSIM	0,94	**0,97**	0,92	0,93	0,94	0,95
	Snr = 10	PSNR	26,67	**29,74**	29,07	29,25	28,41	28,03
		MSE	143,79	**68,38**	79,15	76,51	116,92	111,01
		MSSIM	0,71	0,88	**0,92**	**0,92**	0,82	0,83
		FSIM	0,88	**0,94**	0,83	0,84	0,9	0,91

Table 3 Averaged PSNR, MSE, MSSIM, FSIM evaluation criteria values of 30 liver MR images.

		Evaluation Criteria	Ridgelet	Tetrolet	Wavelet		Curvelet	
					Haar	Db4	First Generation	Second Generation
RANDOM	*Sigma=5*	PSNR	34,47	36,28	34,71	35,30	**39,30**	38,48
		MSE	24,64	8,79	12,91	11,22	**8,14**	10,09
		MSSIM	0,81	0,91	0,90	0,90	**0,95**	0,93
		FSIM	0,85	0,89	0,90	0,90	**0,96**	0,92
	Sigma=10	PSNR	32,01	31,73	30,67	31,54	**36,07**	35,76
		MSE	44,88	25,49	33,98	27,84	**17,53**	19,45
		MSSIM	0,73	0,76	0,77	0,78	**0,91**	0,87
		FSIM	0,82	0,82	0,84	0,86	**0,93**	0,90
	Sigma=15	PSNR	30,86	29,07	28,82	29,60	**34,35**	34,18
		MSE	58,72	47,69	55,08	44,47	**25,73**	27,56
		MSSIM	0,68	0,62	0,67	0,68	**0,87**	0,83
		FSIM	0,80	0,75	0,79	0,82	**0,90**	0,88
GAUSSIAN	*Snr=3*	PSNR	27,16	26,88	27,42	28,26	**33,14**	29,08
		MSE	150,88	114,74	91,62	74,18	**39,47**	98,49
		MSSIM	0,56	0,52	0,58	0,60	**0,82**	0,68
		FSIM	0,78	0,69	0,74	0,78	**0,88**	0,81
	Snr=5	PSNR	27,36	28,46	28,59	29,45	**34,35**	29,01
		MSE	134,68	73,12	69,33	55,27	**31,03**	91,78
		MSSIM	0,6	0,61	0,66	0,67	**0,86**	0,69
		FSIM	0,79	0,74	0,77	0,81	**0,90**	0,80
	Snr=10	PSNR	28,29	30,54	30,13	31,06	**35,66**	30,08
		MSE	107,57	42,77	47,58	36,51	**22,13**	70,72
		MSSIM	0,65	0,72	0,75	0,76	**0,89**	0,74
		FSIM	0,79	0,80	0,88	0,85	**0,92**	0,83
RICIAN	*Snr=3*	PSNR	33,76	35,17	35,12	35,24	**38,06**	37,52
		MSE	28,06	12,46	11,41	11,13	**10,42**	16,7
		MSSIM	0,61	0,78	**0,94**	**0,94**	0,68	0,66
		FSIM	0,87	0,97	0,68	0,68	**0,98**	0,93
	Snr=5	PSNR	31,83	32,09	30,94	31,16	34,08	**36,08**
		MSE	43,64	**25,98**	30,46	29,25	26,59	30,48
		MSSIM	0,52	0,71	**0,91**	**0,91**	0,58	0,57
		FSIM	0,86	**0,97**	0,56	0,57	0,96	0,93
	Snr=10	PSNR	27,13	26,71	25,48	25,66	**28,41**	31,96
		MSE	131,08	**95,13**	113,67	108,68	100,24	107,22
		MSSIM	0,4	0,61	0,85	**0,87**	0,47	0,45
		FSIM	0,82	**0,93**	0,43	0,45	0,92	0,9

Table 4 Averaged PSNR, MSE, MSSIM, FSIM evaluation criteria values of 30 mammography images.

Mammography Images		Evaluation Criteria	Ridgelet	Tetrolet	Wavelet		Curvelet	
					Haar	Db4	First Generation	Second Generation
RANDOM	*Sigma=5*	PSNR	37,06	39,30	37,79	39,14	**40,64**	39,31
		MSE	13,29	6,69	9,64	7,28	**5,73**	9,07
		MSSIM	0,87	0,91	0,90	0,91	**0,95**	0,93
		FSIM	0,90	0,90	0,91	0,92	**0,97**	0,94
	Sigma=10	PSNR	34,56	34,98	34,95	36,02	**37,78**	36,36
		MSE	24,11	18,97	19,51	16,67	**10,85**	15,38
		MSSIM	0,79	0,76	0,80	0,81	**0,91**	0,87
		FSIM	0,86	0,82	0,85	0,88	**0,95**	0,92
	Sigma=15	PSNR	33,06	31,5	33,38	33,63	**36,06**	33,13
		MSE	34,27	44,32	30,68	31,3	**16,58**	32,43
		MSSIM	0,74	0,65	0,7	0,71	**0,89**	0,82
		FSIM	0,84	0,83	0,8	0,84	**0,94**	0,89
GAUSSIAN	*Snr=3*	PSNR	28	22,96	25,54	25,98	**31,14**	28,21
		MSE	111,94	436,47	270,46	235,53	**54,1**	105,06
		MSSIM	0,53	0,25	0,58	0,58	**0,72**	0,63
		FSIM	0,78	0,53	0,3	0,32	**0,89**	0,87
	Snr=5	PSNR	29,1	24,75	27,21	27,73	**32,24**	28,95
		MSE	86,34	262,91	162,5	153,58	**41,76**	88,35
		MSSIM	0,6	0,32	0,39	0,4	**0,77**	0,67
		FSIM	0,81	0,6	0,63	0,65	**0,9**	0,87
	Snr=10	PSNR	30,55	27,58	29,85	29,8	**33,64**	29,99
		MSE	62,83	135,75	81,47	86,89	**29,90**	69,35
		MSSIM	0,64	0,37	0,51	0,52	**0,81**	0,71
		FSIM	0,81	0,57	0,7	0,73	**0,91**	0,88
RICIAN	*Snr=3*	PSNR	35,44	36,78	36,82	37,03	37,95	**38,04**
		MSE	18,83	11,95	11,8	11,28	**10,47**	14,58
		MSSIM	0,63	0,71	**0,95**	0,96	0,67	0,66
		FSIM	0,92	**0,98**	0,66	0,67	**0,98**	0,95
	Snr=5	PSNR	32,92	33,25	32,96	33,37	34,12	**36,16**
		MSE	33,47	27,42	29	27,16	**25,35**	28,28
		MSSIM	0,54	0,61	**0,93**	**0,93**	0,57	0,56
		FSIM	0,9	0,96	0,55	0,56	**0,97**	0,95
	Snr=10	PSNR	27,74	27,65	27,8	28,15	28,42	**31,35**
		MSE	110,37	102,47	102,19	99,87	**94,4**	103
		MSSIM	0,45	0,51	0,86	**0,89**	0,48	0,47
		FSIM	0,87	0,91	0,44	0,46	**0,95**	0,92

Table 5 Averaged PSNR, MSE, MSSIM, FSIM evaluation criteria values of 30 retinal images.

| | | Evaluation Criteria | Ridgelet | Tetrolet | Wavelet | | Curvelet | |
					Haar	Db4	First Generation	Second Generation
RANDOM	*Sigma=5*	PSNR	35,21	**38,46**	37,14	37,47	38,22	37,45
		MSE	19,69	**9,9**	13,46	12,49	**9,9**	11,96
		MSSIM	0,85	0,92	**0,95**	**0,95**	0,92	0,92
		FSIM	0,93	**0,96**	0,9	0,91	0,95	0,95
	Sigma=10	PSNR	32,44	34,58	34,1	33,13	**35,82**	34,42
		MSE	37,29	25,69	28,49	26,4	**17,27**	23,63
		MSSIM	0,77	0,82	**0,9**	0,88	0,89	0,87
		FSIM	0,88	0,91	0,84	0,82	**0,93**	0,92
	Sigma=15	PSNR	30,68	31,93	32,14	32,16	**34,19**	33,09
		MSE	55,96	49,32	47,4	46,1	**24,73**	33,01
		MSSIM	0,72	0,71	0,86	0,87	**0,87**	0,86
		FSIM	0,85	0,84	0,78	0,79	**0,91**	0,9
GAUSSIAN	*Snr=3*	PSNR	22,07	21,47	21,96	23,08	**26,53**	24,3
		MSE	518,24	1092	672,54	595,76	**149,99**	300,61
		MSSIM	0,3	0,13	0,54	0,51	**0,68**	0,57
		FSIM	0,59	0,39	0,24	0,26	**0,81**	0,73
	Snr=5	PSNR	24,9	22,33	23,12	24,28	**27,59**	26,92
		MSE	228,45	625,81	454,17	385,96	**117,19**	138,71
		MSSIM	0,5	0,2	0,58	0,58	**0,72**	0,7
		FSIM	0,72	0,46	0,32	0,34	**0,83**	0,79
	Snr=10	PSNR	26,38	24,46	25,51	26	**28,92**	28,35
		MSE	153,86	332,99	274,93	229,84	**85,93**	96,79
		MSSIM	0,65	0,3	0,66	0,66	**0,76**	0,75
		FSIM	0,79	0,56	0,44	0,46	**0,85**	0,8
RICIAN	*Snr=3*	PSNR	35,96	**39,76**	39,57	39,73	39,73	37,44
		MSE	16,54	7,03	7,53	7,24	**7,02**	11,96
		MSSIM	0,88	0,94	**0,97**	**0,97**	0,94	0,92
		FSIM	0,94	**0,97**	0,93	0,94	0,96	0,94
	Snr=5	PSNR	34,94	**38,05**	36,82	37,09	37,7	36,88
		MSE	20,94	**10,9**	14,51	13,61	11,12	13,96
		MSSIM	0,85	0,92	**0,95**	**0,95**	0,92	0,92
		FSIM	0,93	**0,96**	0,9	0,91	0,95	0,94
	Snr=10	PSNR	30,99	32,81	32,43	32,51	**33,27**	32,8
		MSE	51,88	37,49	41,78	40,57	**30,7**	39,56
		MSSIM	0,76	0,81	0,9	**0,91**	0,87	0,85
		FSIM	0,89	0,92	0,82	0,83	**0,93**	0,91

4. Conclusion

In this study, denoising ability of four MRA techniques are compared. Although the PSNR values are so close to each other for snr=3 for Gaussian noise in Table 2, it is quite obvious that FGCT and SGCT visually outperformed the other transforms in Fig. 5.(a). It means traditional procedures are not adequate enough for evaluation. Results are corroborated with new-generation criteria (MSSIM, FSIM). On the other hand, TT has

overwhelmingly better results than the other transforms for random and rician noisy test images. So, it is clear that TT and CT are suitable methods for denoising studies of benchmark images.

The cleanest results are obtained by FGCT for medical images, visually (Fig.5.(b-d)). Moreover, the almost all best quantita-tive results are also achieved with FGCT. So, the best method for denoising the medical images is FGCT. On the other hand, TT surpasses RT, Haar WT and SGCT for almost all rates of rician noise for both liver MR and fundus images (Table 3, 5). In addition to that, TT gets better results than db4 WT and FGCT as long as the noise rates of liver MR images reduce. Considering that MR images follow a rician distribution noise, TT is more efficient than the others. Lastly, although SGCT has a short process time, FGCT achieves better results than it for almost all types of noise and images.

TT is applied on biomedical images for the first time in literature and it can be an alternative to haar considering the results. Although the performance of TT decreases in high noise rates and takes much more time to perform, generally it has the drop on haar WT. As a future study, different thresholding methods can be applied to improve the performances of the transforms. TT and FGCT have the longest-running processes, so a time-comparative study between these transforms could be realized.

Acknowledgements

References

[1] S. Mallat, "A theory for multiresolution signal decomposition: the wavelet representation,"*IEEE Transactions on Pattern Analysis and Machine Intelligence*, vol. 11, pp. 674–693,1989.

[2] I. Daubechies, "Ten lectures on wavelets",PA: SIAM, Philadelphia, 1992.

[3] M. Lang, H. Guo, J.E. Odegard, C.S. Burrus, R.O. Wells,"Noise reduction using an undecimated discrete wavelet transform,"*IEEE Signal Processing Letters*, vol. 3,pp. 10-12, 1996.

[4] A. Mojsilovic, M. Popovic, D. Sevic, "Classification of the ultrasound liver images with the 2N x 1-D wavelet transform,"*Proceedings of the IEEE International Conference on Image Processing*, Laussanne, Switzerland, 1996,pp. 367-370.

[5] I. Delakis, O. Hammad, R.I. Kitney,"Wavelet-based denoising algorithm for images acquired with parallel magnetic resonance imaging (MRI)," *Physics in Medicine And Biology*, vol. 52, pp. 3741-3751, *2007*.

[6] V. Kidsumran, W. Chiracharit, "Contrast enhancement mammograms using denoising in wavelet coefficients,"*10th International Joint Conference on Computer Science and Software Engineering*, Maha Sarakham, Tayland, 2013, pp. 82-86.

[7] E. Candes, D.L. Donoho, "Ridgelets: the key to high-dimensional intermittency,"*Philosophical Transactions of the Royal Society A*, vol. 357, pp. 2495–2509, 1999.

[8] M.N. Do, M. Vetterli, "The finite ridgelet transform for image representation,"*IEEE Transactions on Image Processing,*vol. 12,pp. 16-28, 2003.

[9] X. Wang, "Wrap-around effect removal finite ridgelet transform for multiscale image denoising,"*Pattern Recognition*, vol. 43, pp. 3693-3698, 2010.

[10] F. Makhlouf, N. Khlifa, H. Besbes, C. B. Amar, B.Soulaiman, "A comparative study of multiresolution methods to reduce the noise in scintigraphic images,"*International Conference on Computer Medical Applications*, Sousse, Tunis, 2013, pp. 1-5.

[11] H. Yaşar, M. Ceylan, A.E. Öztürk, "Comparison of real and complex-valued versions of wavelet transform, curvelet transform and ridgelet transform for medical image denoising,"*IJEMME*, vol.3,pp. 427-436, 2013.

[12] E.J. Candes, D.L. Donoho, "*Curvelets - a surprisingly effective nonadaptive representation for objects with edges*", in: Cohen A, Rabut C, Schumaker LL, eds. Curve and surface fitting: Saint Malo 1999. Nashville: Vanderbilt University Press, 2000.

[13] D.L. Donoho, M.R. Duncan, "Digital curvelet transform: strategy, implementation and experiments,"*Proceedings of SPIE: Wavelet Application VII*, vol. 4056,pp. 12-30, 2000, DOI:10.1117/12.381679.

[14] E.J. Candes,L. Demanet, D.L. Donoho, L. Ying, "Fast discrete curvelet transforms,"*Multiscale Modeling And Simulation*, vol. 5, pp. 861-899, 2006.

[15] J.L. Starck, E.J. Candes, D.L. Donoho, "The curvelet transform for image denoising,"*IEEE Transactions on Image Processing*, vol. 11, pp. 670-684, 2002.

[16] C. Kamath, A. Gyaourova, I.K. Fodor,"Undecimated curvelet transforms for image denoising", Center for Applied Scientific Computing, Lawrencelivermore National Laboratory, Tech. Rep. UCRL-ID-150931,2002.

[17] R. Sivakumar, "Denoising of computer tomography images using curvelet transform",*ARPN Journal of Engineering and Applied Sciences*, vol. 2,pp. 21-26, 2007.

[18] J. Ma, G. Plonka, "The curvelet transform - a review of recent applications,"*IEEE Signal Processing Magazine*, vol. 27,pp. 118-133, 2010.

[19] E. Malar, A. Kandasamy, S.S. Kirthana, D. Nivedhitha, "A comparative study on mammographic image denoising technique using wavelet, curvelet and contourlet transforms,"*International Conference on Machine Vision And Image Processing*, Nadu, India, 2012,pp. 65-68.

[20] S. AlZubi, N. İslam, M. Abbod, "Multi-resolution analysis using curvelet and wavelet transforms for medical imaging,"*Medical Measurements and Applications Proceedings*, Bari, Italy, 2011,pp. 188-191.

[21] V. V. K. Raju, M. P. Kumar, "Denoising of MRI and X-ray images using dual tree complex wavelet and curvelet transforms,"*International Conference on Communication and Signal Processing*, Melmaruvathur, India, 2014,pp. 1844-1848.

[22] J. Krommweh, "Tetrolet transform: a new adaptive haar wavelet algorithm for sparse image representation,"*Journal of Visual Communication And Image Representation*, vol. 21,pp. 364-374, 2010.

[23] M.K. Singh, "Denoising of natural images using the wavelet transform," M.S. thesis, San Jose State University, 2010.

[24] P. Jain, V. Tyagi, "An adaptive edge-preserving image denoising technique using tetrolet transforms,"*The Visual Computer*, vol. 31,pp. 657-674, 2014.

[25] M. Ceylan, A.E. Öztürk, "Determining the number of tetrominoe orders for denoising applications performed by tetrolet transform,"*IEEE 22nd Signal Processing and Communications Applications Conference*, Trabzon, Turkey,2014, pp. 216-219(in Turkish).

[26] M.M.R. Mohan, V.S. Sheeba, "A novel method of medical image denoising using bilateral and NLM filtering,"*3rd International Conference on Advances in Computing and Communications*, Cochin, India, 2013, pp. 186-191.

[27] H. Yu, L. Zhao, "An efficient denoising procedure for magnetic resonance imaging,"*The 2nd International Conference on Bioinformatics and Biomedical Engineering*, Shangai, China, 2008, pp. 2628-2630.

[28] V. N. P. Raj, T.Venkateswarlu, "Denoising of MR images using adaptive multiresolution subband mixing,"*IEEE International*

Conference on Computational Intelligence and Computing Research, Enathi, India, 2013, pp. 1-6.

[29] S. Li, H. Yin, L. Fang, "Group-sparse representation with dictionary learning for medical image denoising and fusion,"*IEEE Transactions on Biomedical Engineering*, vol. 59, pp. 3450-3459, 2012.

[30] S. Bhatnagar, R.C. Jain, "Different denoising techniques for medical images in wavelet domain,"*International Conference on Signal Processing and Communication*, Noida, India, 2013,pp. 325-329.

[31] L. Dai, Y. Zhang,Y. Li, "Image denoising using BM3D combining tetrolet prefiltering,"*Information Technology Journal*, vol. 12, pp. 1995-2001, 2013.

[32] Z. Wang, A.C. Bovik, H.R. Sheikh, E.P. Simoncelli, "Image quality assessment: from error measurement to structural similarity,"*IEEE Transactions on Image Processing*, vol. 13,pp. 600-612, 2004.

[33] D. Brunet, E.R. Vrscay, Z. Wang, "On the mathematical properties of the structural similarity index,"*IEEE Transactions on Image Processing*, vol. 21, pp. 1488-1499, 2012.

[34] N. Thakur, S. Devi, "A new method for color image quality assessment,"*International Journal of Computer Applications*, vol. 15,pp. 10-17, 2011.

[35] L. Zhang, L. Zhang, X. Mou, D. Zhang, "FSIM: a feature similarity index for image quality assessment,"*IEEE Transactions on Image Processing*, vol. 20,pp. 2378-2386, 2011.

[36] J. Suckling, J. Parker, D.R. Dance, S. Astley, I. Hutt, C. Boggis, I. Ricketts, E. Stamatakis, N. Cerneaz, S.L. Kok, P. Taylor, D. Betal, J. Savage, *"*The Mammographic Image Analysis Society Digital Mammogram Database",*International Congress Series*, vol. 1069,pp. 375-378, 1994.

[37] J.J. Staal, M.D. Abramoff, M. Niemeijer, M.A. Viergever, B.V. Ginneken, "Ridge based vessel segmentation in color images of the retina,"*IEEE Transactions on Medical Imaging*, vol. 23,pp. 501-509, 2004.